Dioxygenase-encoding *AtDAO1* gene controls IAA oxidation and homeostasis in *Arabidopsis*

Silvana Porco[a,1,2], Aleš Pěnčík[b,c,d,1], Afaf Rashed[a,1], Ute Voß[a,1], Rubén Casanova-Sáez[b,1], Anthony Bishopp[a], Agata Golebiowska[a,e], Rahul Bhosale[a], Ranjan Swarup[a], Kamal Swarup[a], Pavlína Peňáková[c,d], Ondřej Novák[b,c,d], Paul Staswick[f], Peter Hedden[g], Andrew L. Phillips[g], Kris Vissenberg[e], Malcolm J. Bennett[a,3,4], and Karin Ljung[b,3,4]

[a]Centre for Plant Integrative Biology, Plant and Crop Science Division, School of Biosciences, University of Nottingham, Loughborough LE12 5RD, United Kingdom; [b]Umeå Plant Science Centre, Department of Forest Genetics and Plant Physiology, Swedish University of Agricultural Sciences, SE-901 83 Umea, Sweden; [c]Laboratory of Growth Regulators, Centre of the Region Haná for Biotechnological and Agricultural Research, Institute of Experimental Botany Academy of Sciences of the Czech Republic (AS CR), CZ-78371 Olomouc, Czech Republic; [d]Faculty of Science, Palacký University, CZ-78371 Olomouc, Czech Republic; [e]Integrated Molecular Plant Physiology Research, Biology Department, Antwerp University, 2020 Antwerp, Belgium; [f]Department of Agronomy and Horticulture, University of Nebraska, Lincoln, NE 68583-0915; and [g]Department of Plant Biology and Crop Science, Rothamsted Research, Hertfordshire AL5 2JQ, United Kingdom

Edited by Mark Estelle, University of California at San Diego, La Jolla, CA, and approved July 26, 2016 (received for review March 22, 2016)

Auxin represents a key signal in plants, regulating almost every aspect of their growth and development. Major breakthroughs have been made dissecting the molecular basis of auxin transport, perception, and response. In contrast, how plants control the metabolism and homeostasis of the major form of auxin in plants, indole-3-acetic acid (IAA), remains unclear. In this paper, we initially describe the function of the *Arabidopsis thaliana* gene *DIOXYGENASE FOR AUXIN OXIDATION 1* (*AtDAO1*). Transcriptional and translational reporter lines revealed that *AtDAO1* encodes a highly root-expressed, cytoplasmically localized IAA oxidase. Stable isotope-labeled IAA feeding studies of loss and gain of function *AtDAO1* lines showed that this oxidase represents the major regulator of auxin degradation to 2-oxoindole-3-acetic acid (oxIAA) in *Arabidopsis*. Surprisingly, *AtDAO1* loss and gain of function lines exhibited relatively subtle auxin-related phenotypes, such as altered root hair length. Metabolite profiling of mutant lines revealed that disrupting *AtDAO1* regulation resulted in major changes in steady-state levels of oxIAA and IAA conjugates but not IAA. Hence, IAA conjugation and catabolism seem to regulate auxin levels in *Arabidopsis* in a highly redundant manner. We observed that transcripts of *AtDOA1* IAA oxidase and *GH3* IAA-conjugating enzymes are auxin-inducible, providing a molecular basis for their observed functional redundancy. We conclude that the *AtDAO1* gene plays a key role regulating auxin homeostasis in *Arabidopsis*, acting in concert with *GH3* genes, to maintain auxin concentration at optimal levels for plant growth and development.

Arabidopsis thaliana | IAA degradation | oxidase | dioxygenase | root hair elongation

Distinct indole-3-acetic acid (IAA) conjugation and degradation pathways operate to maintain optimal auxin concentrations for plant growth and developmental processes. There are three major forms of auxin conjugates identified in diverse plants: ester-linked IAA-sugar conjugates, amide-linked IAA-amino acid conjugates, and amide-linked IAA peptide and protein conjugates (reviewed in ref. 1). In *Arabidopsis thaliana*, Group II of the Gretchen Hagen3 (GH3) family of auxin-inducible acyl amido synthetases converts IAA to IAA-amino acids (2, 3). Most amino acid IAA conjugates are believed to be inactive; however, there are enzymes that can hydrolyze some of the IAA-amino acid conjugates to free IAA (reviewed in ref. 1). Some of the IAA-amino acid conjugates, such as indole-3-acetic acid aspartic acid (IAA-Asp) and indole-3-acetic acid glutamic acid (IAA-Glu), can also be further metabolized (4–6). The conversion of IAA to indole-3-acetic acid glucose (IAA-glc) is catalyzed by the UDP glucosyltransferase UGT84B1 (7).

The major IAA catabolite in *Arabidopsis* is 2-oxoindole-3-acetic acid (oxIAA), the oxidized form of IAA (4, 6, 8). oxIAA can be further metabolized by conjugation to glucose (4, 5), and it was recently shown that the UDP glucosyltransferase UGT74D1 is able to catalyze the glucosylation of oxIAA to 2-oxoindole-3-acetic acid glucose (oxIAA-glc) (9). IAA catabolism has been shown to be an irreversible step (4, 10), and the oxIAA product has very little biological activity and is not transported via the polar auxin transport system (6, 8).

Although many metabolites in the conjugation and catabolic pathways have been identified in *Arabidopsis* (4–7, 9–11), it has proved difficult to identify and characterize the genes and enzymes involved. We have now identified two closely related components of the IAA degradation machinery in *Arabidopsis*, *DIOXYGENASE FOR AUXIN OXIDATION 1* (*AtDAO1*; *At1g14130*) and *AtDAO2* (*At1g14120*), which are closely related to genes described in apple [*Adventitious Rooting Related Oxygenase 1* (12)] and rice [*DAO* (13)]. The *AtDAO1* and *AtDAO2* genes belong to a distinct clade of the 2-oxoglutarate–dependent dioxygenase gene family and are related to enzymes involved in gibberellin biosynthesis and inactivation. We report that the *AtDAO1* gene plays a key role regulating auxin homeostasis in *Arabidopsis*, acting in concert with *GH3* genes to maintain auxin concentration at optimal levels for plant growth and development. As a result, plants lacking *AtDAO1* activity led to

Significance

Understanding how hormones like auxin control plant growth and development has fascinated scientists since Darwin. The past two decades have seen breakthroughs in elucidating the molecular basis of auxin transport, perception, and response, but little is known about how auxin is metabolized or its homeostasis is controlled. We report that the *DIOXYGENASE FOR AUXIN OXIDATION 1* (*AtDAO1*) enzyme represents the major pathway for auxin oxidation in *Arabidopsis*. Disrupting *AtDAO1* function elevates levels of auxin conjugates between ∼50- and 280-fold, but auxin levels remain close to the WT, helping explain why mutant phenotypes are relatively weak. We conclude that *AtDAO1* and auxin conjugation pathways play highly redundant roles and reveal a level of regulation of auxin abundance in plants.

Author contributions: S.P., A.P., A.R., U.V., R.C.-S., O.N., M.J.B., and K.L. designed research; S.P., A.P., A.R., U.V., R.C.-S., A.B., A.G., R.B., R.S., K.S., P.P., and O.N. performed research; P.S. contributed new reagents/analytic tools; S.P., A.P., A.R., U.V., R.C.-S., A.B., A.G., R.B., R.S., K.S., P.P., O.N., P.H., A.L.P., and K.V. analyzed data; and M.J.B. and K.L. wrote the paper.

The authors declare no conflict of interest.

This article is a PNAS Direct Submission.

Freely available online through the PNAS open access option.

[1]S.P., A.P., A.R., U.V., and R.C.-S. contributed equally to this work.

[2]Present address: Department of Cell and Molecular Biology, The Scripps Research Institute, La Jolla, CA 92037.

[3]M.J.B. and K.L. contributed equally to this work.

[4]To whom correspondence may be addressed. Email: malcolm.bennett@nottingham.ac.uk or karin.ljung@slu.se.

This article contains supporting information online at www.pnas.org/lookup/suppl/doi:10.1073/pnas.1604375113/-/DCSupplemental.

major changes in conjugated forms of the hormone, but auxin level remains within a normal range, helping explain why the mutant exhibited subtle phenotypic changes. We conclude that IAA catabolism and conjugation regulate auxin homeostasis in *Arabidopsis* in a highly redundant manner.

Results

IAA Oxidation in *Arabidopsis* Is Controlled by the Dioxygenase Gene *AtDAO1*. To study the in vivo formation of IAA metabolites, a feeding experiment was performed using [$^{13}C_6$]IAA with WT *Arabidopsis* seedlings. We observed rapid labeling of the pools of the major IAA conjugates IAA-Asp, IAA-Glu, and IAA-glc as well as the catabolites oxIAA and oxIAA-glc within 3 h after treatment began, revealing that IAA is rapidly turned over in *Arabidopsis* seedlings (Fig. 1*A*).

A rice *DAO1* gene that encodes a 2-oxoglutarate–dependent Fe (II) dioxygenase-like enzyme has recently been reported to mediate IAA oxidation (13). Phylogenetic analyses revealed that the *Arabidopsis* genome contains two genes related to *OsDAO1* termed *At1g14130* (*AtDAO1*) and *At1g14120* (*AtDAO2*). *AtDAO1* and *AtDAO2* belong to the 2-oxoglutarate–dependent Fe (II) dioxygenase gene family, and their sequences are related to enzymes involved in gibberellin biosynthesis and inactivation (Fig. S1*A*). A BLAST search of the sequenced plant genomes at Phytozome (https://phytozome.jgi.doe.gov/pz/portal.html) identified sequences closely related to *AtDAO1* and *AtDAO2* in a range of species, with amino acid identities ranging from 47 to 93% (Fig. S1*B*).

To address the putative IAA oxidative role of *AtDAO1* in *Arabidopsis*, we identified several Transfer-DNA (T-DNA) insertion lines (Fig. 1*B*). The T-DNA for the Salk_093162 line (*dao1-1*) is inserted in the first exon of At1g14130 311 bp downstream of the start codon. Sail line 349_D02 (*dao1-2D*) has a T-DNA insertion in the intergenic region between the *AtDAO1* and *AtDAO2* genomic sequences 542 bp upstream of the *AtDAO2* start codon. T-DNA insertions in Salk_082522 (*dao1-3*) and Salk_095931 (*dao1-4D*) lines are positioned upstream of the start codon of *AtDAO1* (591 and 789 bp, respectively). Quantitative RT-PCR (qRT-PCR) was performed to measure transcript levels of *DAO1* and *DAO2* in the T-DNA lines (Fig. S2*A*). *DAO1* mRNA was strongly reduced in *dao1-1* and *dao1-3* lines, suggesting that they represent loss of function lines. In contrast, for *dao1-2D* and *dao1-4D* lines, *AtDAO1* mRNA abundances were 4- and 2.4-fold higher than the WT, respectively, suggesting that they represent *AtDAO1* overexpressing lines. No significant changes were detected in the expression level of *DAO2* in any of these lines compared with in the WT (Fig. S2*A*).

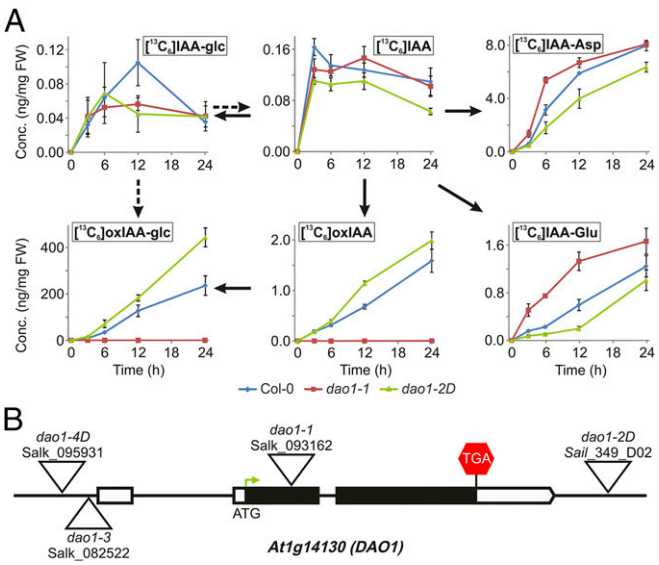

Fig. 1. IAA oxidation in *Arabidopsis* is regulated by the dioxygenase gene family member *At1g14130* (*AtDAO1*). (*A*) IAA feeding experiment. Formation of labeled IAA conjugates and catabolites after incubation of 7-d-old *Arabidopsis* Col-0, *dao1-1*, and *dao1-2D* seedlings with [$^{13}C_6$]IAA. Samples were analyzed in three independent biological replicates. Error bars represent SD. FW, fresh weight. (*B*) Structure of the *Arabidopsis DAO1* gene with indication of the position of the T-DNA insertions (triangles) in the different *dao1* alleles studied.

The [$^{13}C_6$]IAA feeding experiments were also performed using seedlings from *dao1-1* (*AtDAO1* mutant) and *dao1-2D* (*AtDAO1* overexpressing) lines, revealing that (unlike the WT and *dao1-2D*) *dao1-1* seedlings failed to oxidize [$^{13}C_6$]IAA to [$^{13}C_6$]oxIAA (Fig. 1*A*). Formation of [$^{13}C_6$]oxIAA-glc was also abolished in the *dao1-1* mutant line. Instead, ^{13}C-labeled IAA was converted to IAA conjugates ([$^{13}C_6$]IAA-Asp and [$^{13}C_6$]IAA-Glu) at a higher rate than in WT seedlings. Conversely, the *dao1-2D* line oxidized [$^{13}C_6$]IAA to [$^{13}C_6$]oxIAA and [$^{13}C_6$]oxIAA-glc more rapidly than the WT, and the [$^{13}C_6$]IAA conjugate levels were diminished in this line. Labeling of IAA-glc is similar in all lines, suggesting that the formation of this conjugate is not altered in *AtDAO1* mutant and overexpressing lines (Fig. 1*A*). Hence, our [$^{13}C_6$]IAA feeding experiments revealed that *AtDAO1* plays an essential role regulating IAA oxidation in *Arabidopsis* seedlings.

Mutants Disrupting *AtDAO1* Activity Exhibit Subtle Changes in Shoot and Root Phenotypes. We next characterized the phenotypes of the *dao1* mutants (Fig. 2). Given the apparent importance of *AtDAO1* mediating IAA oxidation in *Arabidopsis* seedlings (Fig. 1*A*), we expected mutant and overexpressing plants to exhibit multiple IAA-related developmental defects. Surprisingly, *AtDAO1* mutant and overexpressing lines exhibited only mild defects in plant growth and development (Fig. 2). Compared with WT seedlings, *AtDAO1* mutant lines exhibit a slight reduction in primary root length and increase in lateral root density (Fig. 2*A* and Fig. S3 *A* and *B*). The root gravitropic response was faster in loss of function *dao1-1* and *dao1-3* mutants compared with in *dao1-2D* and *dao1-4D*, with response that was similar to that in the WT (Fig. S3*C*). In shoot tissues, increased branching and shorter siliques were observed in *dao1-1*, whereas *dao1-2D* adult plants exhibited a growth phenotype closer to the WT (Fig. 2 *B* and *C*).

Our root hair (RH) measurements revealed that their length increased ~80% in *dao1-1* and *dao1-3* seedlings compared with the WT (Fig. 2 *D* and *E*). RH determination and elongation in *Arabidopsis* is controlled (in part) by a small family of basic Helix-Loop-Helix transcription factors that includes the auxin-inducible gene member *RSL4* (14–16). Datta et al. (17) have recently shown that RH length is proportional to *RSL4* mRNA abundance. Significantly, qRT-PCR analysis revealed that *dao1-1* and *dao1-3* seedlings contained an ~80% increase in *RSL4* transcript levels (Fig. 2*F*), which is directly proportional to their altered RH length. Interestingly, multicellular root modeling predicts an accumulation of IAA in epidermal tissues in the *dao1-1* mutant (18), and the RH phenotype in *dao1-1* and *dao1-3* (Fig. 2 *D* and *E*) supports the model. We conclude that, despite the importance of *AtDAO1* controlling auxin oxidation (Fig. 1*A*), loss and gain of function lines exhibit surprisingly weak auxin-related phenotypic alterations (Fig. 2). Nevertheless, *dao1-1* primary root length, lateral root density, and lateral root length were all more sensitive to external IAA treatments than the WT or *dao1-2D* (Fig. S3 *D*–*F*), consistent with the *dao1-1* mutant having a reduced ability to break down auxin.

***AtDAO1* Encodes a Root-Expressed Cytoplasmically Localized IAA Oxidase.** To determine whether the mild *dao1* RH phenotype (Fig. 2 *D*–*F*) could be caused by an RH-specific expression

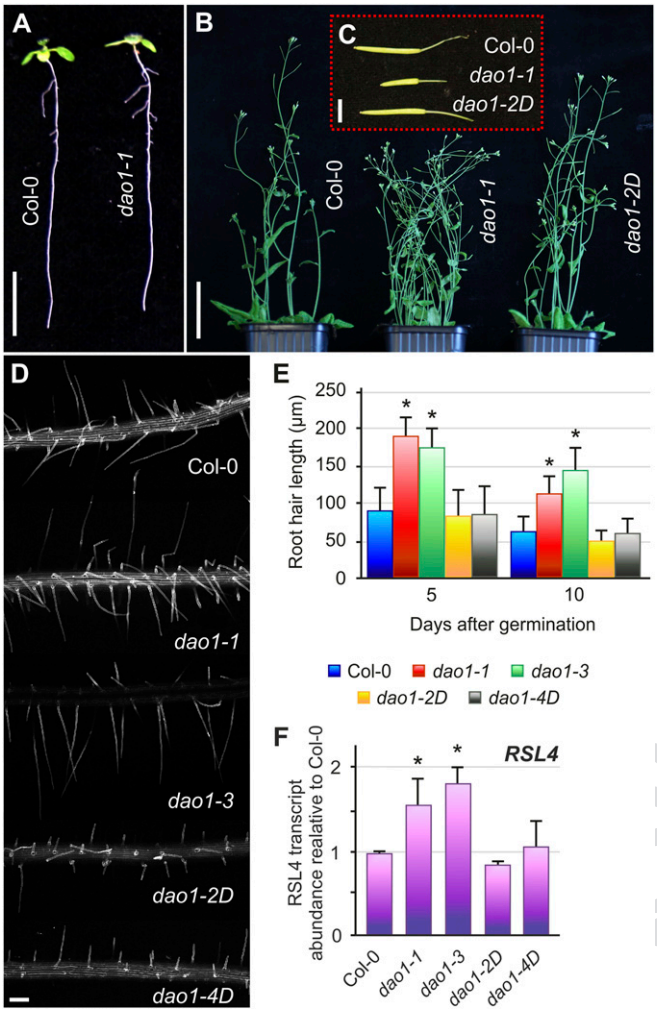

Fig. 2. Developmental phenotypes of *dao1* mutants. (*A*) Seedlings from Col-0 and the *dao1-1* mutant 10 d after germination. (*B*) Adult Col-0, *dao1-1*, and *dao1-2D* plants. (*C*) Mature siliques from plants in *B*. (*D*) Confocal images showing propidium iodide-stained mature RHs from the root tip of 10-d-old Col-0 and *dao1* alleles. (*E*) RH length from 5- and 10-d-old Col-0 and *dao1* alleles. *Values significantly different from those in Col-0 (Mann–Whitney *U* test; $P < 0.001$; $n = 10$). (*F*) qRT-PCR analysis of the expression of the *RSL4* gene in roots from Col-0 and *dao1* alleles harvested 7 d after germination. Error bars indicate SDs from three biological replicates. *Expression values significantly different from those in Col-0 (Student's *t* test; $P < 0.05$). (Scale bars: *A*, 1 cm; *B*, 5 cm; *C*, 5 mm; *D*, 120 μm.)

pattern, we created a transcriptional fusion of At1g14130 (*AtDAO1*) with the β-glucuronidase (GUS) reporter (*pDAO1:GUS*) (Fig. S4). Histochemical staining of transgenic *pDAO1:GUS* seedlings revealed reporter activity in the root tip and vascular (stele) tissues (Fig. S4 *A*, *C*, and *G*). In addition, GUS was detected in epidermal cells in the mature part of the root differentiation zone (Fig. S4*D*), including RHs (Fig. S4 *E* and *F*). In contrast, no GUS expression was observed in lateral root (LR) primordia (Fig. S4*D*) or aerial tissues (Fig. S4*B*).

To investigate whether DAO1 stability is subject to posttranslational regulation, transgenic *Arabidopsis* plants expressing a GFP translational fusion to the At1g14130 genomic sequence (p*DAO1::DAO1-GFP*) were engineered. Confocal microscopy revealed that the DAO1-GFP fusion protein was detected throughout root apical (Fig. 3*A*) and mature tissues, including RHs (Fig. 3 *B* and *E*). The spatial expression pattern of *DAO1* is similar in a transcriptional reporter (*pDAO1:GUS*) (Fig. S4) as it is in a translational fusion (*pDAO1:DAO1-GFP*) (Fig. 3), suggesting that the pattern is largely controlled at the transcriptional level. Higher-magnification confocal images of the p*DAO1::DAO1-GFP* expressing root cells revealed that the IAA oxidase is localized in the cytoplasm and probably excluded from nuclei and central vacuole compartments (Fig. 3 *C*–*E*).

IAA Metabolite Profiling Reveals That *AtDAO1* Regulates oxIAA Levels in *Arabidopsis*. To study the effect of the *AtDAO1* gene on auxin homeostasis, we performed IAA metabolite profiling of *dao1-1* mutant and *dao1-2D* overexpressing lines. Using liquid chromatography–tandem MS (LC-MS/MS) analysis (11), we quantified free IAA and the major IAA precursors, catabolites, and conjugates in 7-d-old seedlings of WT Columbia-0 (Col-0), *dao1-1*, and *dao1-2D*.

In *dao1-1* and *dao1-2D*, the concentrations of IAA and the IAA precursors tryptophan (TRP), anthranilate, and indole-3-acetaldoxime were not significantly affected (Fig. S5). However, the IAA precursors indole-3-acetamide, indole-3-pyruvic acid, and indole-3-acetonitrile were significantly reduced in these lines compared with in the WT (Fig. S5). We also quantified IAA conjugates and catabolites in *dao1-1* and *dao1-2D* seedlings and observed a significant reduction of oxIAA and oxIAA-glc levels in *dao1-1* as well as a significant increase in oxIAA and oxIAA-glc levels in *dao1-2D*, confirming that *dao1-1* and *dao1-2D* behave as KO and overexpressing lines, respectively (Fig. 4). In contrast, the levels of IAA-glc were not changed in these lines. In a second experiment, we performed IAA metabolite profiling of

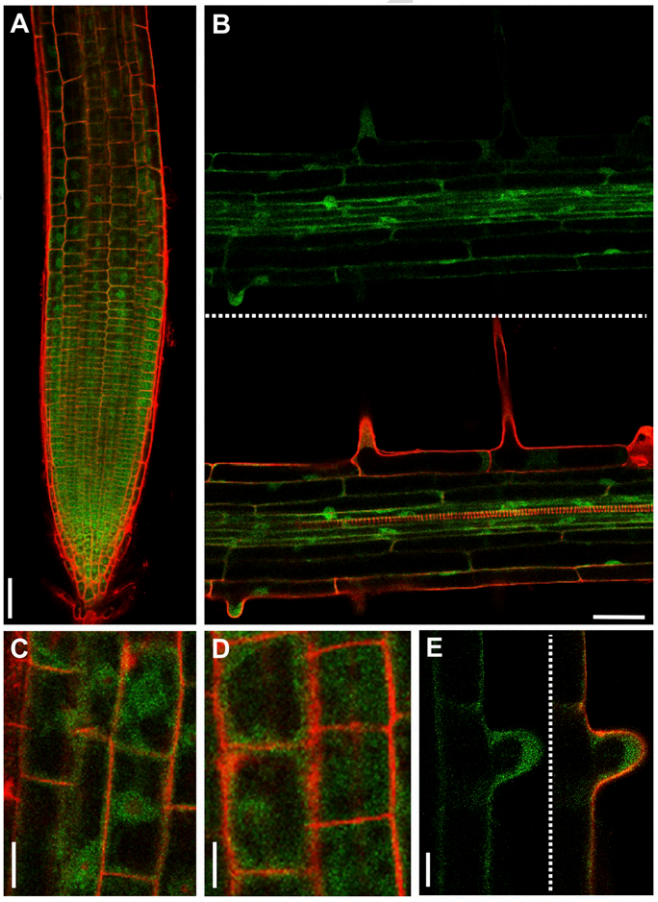

Fig. 3. Cellular localization of DAO1-GFP in roots. Confocal images of root cells from 5-d-old transgenic *pDAO1::DAO1-GFP* plants, showing (*A*) root tip epidermal cells, (*B*) section of the root vasculature in the mature root region, (*C* and *D*) magnification of cells from *A*, and (*E*) magnification of a trichoblast from *B*. Green and red signals correspond to GFP and propidium iodide, respectively. (Scale bars: *A* and *B*, 50 μm; *C* and *D*, 10 μm; *E*, 25 μm.)

all *DAO1* mutant and overexpressing lines compared with the Col-0 WT. The profiles were very similar between the two mutant (*dao1-1* and *dao1-3*) as well as between the two overexpressing (*dao1-2D* and *dao1-4D*) lines (Fig. S2*B*).

Strikingly, a major up-regulation of the IAA amino acid conjugates IAA-Asp and IAA-Glu was observed in *dao1-1* compared with the WT (around ~280- and 46-fold, respectively) (Fig. 4). In contrast, the oxidase overexpressing line *dao1-2D* exhibited significantly reduced levels of IAA-Glu and IAA-Asp (Fig. 4). This discovery prompted us to quantify IAA metabolites in a mutant line disrupting IAA amino acid conjugation. The *GH3* sextuple mutant *gh3.1,2,3,4,5,6*, which comprises six of eight IAA-amino acid–conjugating enzyme genes, exhibited a significant increase in IAA and its precursor TRP (Fig. S5). However, levels of oxIAA, oxIAA-glc, and IAA-glc were not affected compared with Col-0, but the levels of IAA-Asp were below the detection limit, whereas the IAA-Glu levels were significantly elevated (Fig. 4). This increase is most likely caused by the IAA-conjugating activity of GH3.17, which prefers Glu over other amino acids, whereas GH3 1–6 exhibits activity with Asp (2, 3). The *gh3.1,2,3,4,5,6* mutant line also has a stronger auxin overproduction phenotype compared with the mild auxin overproduction phenotype in *dao1-1*, with increased lateral root formation and elongated petioles (Fig. S6).

IAA metabolite profiling different tissues of 10-d-old seedlings revealed similar changes in metabolite distribution in every WT and *dao1-1* tissue analyzed (Fig. S7). We conclude that disrupting *AtDAO1* caused major changes in steady-state levels of oxIAA, oxIAA-Glc, and IAA conjugates but only minor changes in IAA levels (Fig. 4 and Figs. S2*B* and S7).

IAA Conjugation and Catabolism Redundantly Regulate IAA Homeostasis. To monitor the rates of de novo synthesis of these metabolites, a feeding experiment was performed using [$^{15}N_1$]indole as IAA precursor. IAA as well as IAA conjugates and catabolites were rapidly labeled after incubation (Fig. S8). The *gh3.1,2,3,4,5,6* line exhibited the most rapid labeling of IAA, consistent with a higher IAA synthesis rate and/or lower turnover via conjugation. Labeling of oxIAA and oxIAA-glc was highest in *dao1-2D* and lowest in *dao1-1* as expected in IAA oxidase overexpressing and IAA oxidase mutant lines, respectively. In contrast, extremely rapid labeling of IAA-Asp and IAA-Glu was observed in *dao1-1*, indicating that the high endogenous IAA conjugate levels observed (Fig. 4 and Figs. S2*B* and S7) originate from de novo synthesis.

We also quantified IAA metabolites in two *35S:DAO1* lines (Fig. S9). In these constitutive IAA oxidase overexpressing lines, we could not observe any significant changes in IAA and oxIAA levels compared with in the WT. However, a significant up-regulation of both oxIAA-glc and IAA-glc was detected in one of the *35S:DAO1* lines, suggesting that glucosylation pathways were active, whereas the levels of IAA-Asp and IAA-Glu were strongly down-regulated in both *35S:DAO1* lines (Fig. S9). Hence, IAA metabolite profiling has revealed that IAA conjugation and catabolism regulate IAA homeostasis redundantly in *Arabidopsis* seedlings.

Previously described components of the IAA homeostasis machinery, such as *GH3* genes, have been described to be rapidly auxin inducible (1). Transcript profiling of auxin-treated root apical tissues revealed that, like *GH3* genes, *AtDAO1* was auxin inducible, albeit with a lower level of induction and on a longer timescale >4 h (18).

IAA metabolite profiling of *AtDAO1* and *GH3* mutant lines has revealed that IAA conjugation and catabolism regulate auxin homeostasis redundantly (Fig. 4). Given that IAA-Asp and IAA-Glu were present at high levels in the *dao1-1* mutant, we measured the expression of *GH3.2* and *GH3.3* genes in the *dao1-1* and *dao1-2D* mutant backgrounds (Fig. S10). A 1.8-fold increase in gene expression was detected for *GH3.3* in the *dao1-1* mutant compared with in the WT. In contrast, *GH3.3* expression was down-regulated in the *dao1-2D* overexpressor line (Fig. S10). We conclude that auxin-inducible expression of both *AtDOA1* and *GH3* genes could provide a molecular mechanism to explain the observed functional redundancy in IAA catabolism and conjugation that regulates auxin homeostasis.

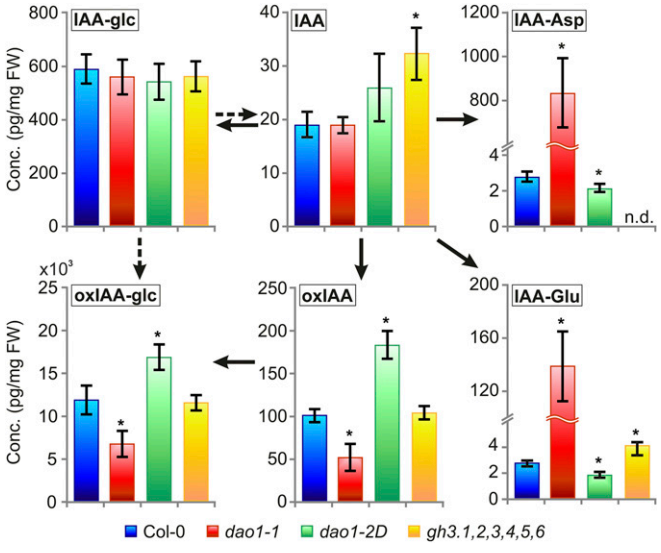

Fig. 4. Levels of IAA metabolites in IAA oxidase and *GH3* sextuple mutant lines. IAA and the metabolites oxIAA, oxIAA-glc, IAA-glc, IAA-Asp, and IAA-Glu were quantified in 7-d-old seedlings of Col-0, *dao1-1*, *dao1-2D*, and the *gh3* sextuple mutant line *gh3.1,2,3,4,5,6*. The concentrations for all metabolites except oxIAA-glc [nanograms per milligram fresh weight (FW)] are given in picograms per milligram FW. Samples were analyzed in five independent biological replicates, and error bars represent the SD. *Statistically significant differences from Col-0 ($P < 0.05$; Student's *t* test).

Discussion

Maintaining auxin homeostasis is critical for growth and developmental processes in plants. Several mechanisms have been proposed to control auxin homeostasis, including IAA metabolism (biosynthesis, degradation, and conjugation), transport, and compartmentation (reviewed in ref. 19). In this paper, we initially describe the key gene regulating IAA oxidation in *Arabidopsis*, *AtDAO1*. In parallel, Zhang et al. (20) have shown that the recombinant *AtDAO1* protein (and the closely related *AtDAO2* sequence) has IAA oxidase activity in vitro. Confocal imaging of GFP-tagged AtDAO1-expressing transgenic plants suggests that the IAA oxidase is localized cytoplasmically (Fig. 3) and based on subcellular fractionation studies (20), behaves as a soluble protein.

In planta stable isotope-labeled auxin feeding studies have revealed the critical importance of AtDAO1 converting IAA to oxIAA in *Arabidopsis* seedlings (Fig. 1). In contrast, the in planta role of *AtDAO2* is currently less clear given that oxidation of [$^{13}C_6$]IAA to [$^{13}C_6$]oxIAA and [$^{13}C_6$]oxIAA-glc was completely blocked in the *dao1-1* loss of function mutant (Fig. 1*A*). A clue comes from transcript profiling results by Zhang et al. (20), which reported that *AtDAO1* is widely expressed in root and shoot tissues at much higher levels than *AtDAO2*. In addition, transcriptomic profiling revealed that *AtDAO1* and *AtDAO2* exhibit auxin and circadian regulated patterns of expression, respectively (18,21). Hence, the *Arabidopsis AtDAO* sequences seem to have subfunctionalized since their tandem duplication event, with *AtDAO1* functioning as the major IAA oxidase at the seedling stage of development.

Given how widely the IAA oxidase *AtDAO1* is expressed across root and shoot tissues, loss of function *dao1* mutant alleles exhibit surprisingly subtle auxin-related developmental defects (Fig. 2 and Fig. S3) (20). This observation can be explained in part, following metabolite profiling and modeling studies (Fig. 4)

(18), by IAA oxidation and conjugation pathways regulating auxin homeostasis in a redundant manner. For example, loss of *AtDAO1* expression leads to up-regulation of *GH3* genes (such as *GH3.3*) (Fig. S10), increasing concentrations of IAA conjugates IAA-Asp and IAA-Glu (Fig. 4) that maintain IAA homeostasis (Fig. 5). Nevertheless, *dao1-1* mutant plants exhibit subtle but clear phenotypes (Fig. 2) (20). These data indicate that, although homeostatic mechanisms regulating IAA levels in *Arabidopsis* act redundantly, they cannot fully compensate for the loss of *AtDAO1* (or *GH3*) expression, resulting in auxin-related mutant phenotypes (Fig. 2 and Figs. S3 and S6) (20).

Materials and Methods

Growth Conditions. Seeds were surface sterilized with 50% (vol/vol) hypochlorous acid for 5 min and then, washed three times with sterile deionized water. For IAA metabolite profiling experiments, plant seeds were plated in Murashige and Skoog medium (4.4 g salts per 1 L), including 1% sucrose and 0.5 g/L MES monohydrate, at pH 5.7 and solidified with 0.8% Plant Agar (Duchefa). Seeds were stratified at 4 °C for 72 h in the dark to synchronize germination and then, incubated vertically in a culture room under long-day (LD) conditions (16 h light at 22 °C and 8 h dark at 18 °C; 150 μmol m^{-2} s^{-1}) and at a relative humidity of 67%. For the rest of the experiments, seeds were plated on 1/2 Murashige and Skoog medium (2.17 g salts per 1 L) without sucrose, stratified at 4 °C for 2–3 d, and then, incubated vertically in a culture room at 22 °C under continuous light (120–150 μmol m^{-2} s^{-1}).

Plant Material. The *Arabidopsis* ecotype Columbia was used as the WT in all experiments. The *dao1* T-DNA insertion mutants were obtained from Nottingham *Arabidopsis* Stock Centre, and the insertion was confirmed by PCR using forward and reverse primers in combination with LBb1.3 (for *dao1-1*, *dao1-3*, and *dao1-4D*) or LB1 (for *dao1-2D*) (Table S1). The *gh3* sextuple mutant (*gh3.1,2,3,4,5,6*) was assembled by repeated rounds of crossing between the single-gene insertion mutants or their double- or triple-mutant derivatives. Mutants *gh3.1* and *gh3.2* are in the Landsberg *erecta* background, and primers for their genotyping were previously described (2). All other mutants were in the Col-0 background; *gh3.5* was described previously as *wes1* (22), and *gh3.4* and *gh3.6* are T-DNA insertion lines (Salk_102549 and Salk_013458, respectively), whereas *gh3.3* is a transposon line (SM.37350). Genotyping of *gh3* insertions was done with forward and reverse primers along with Lba1 (for *gh3.4*, *gh3.5*, and *gh3.6*) or 3′dSpm (for *gh3.3*) (Table S1). Each single mutant was verified to be essentially a complete KO by Northern blot hybridizations.

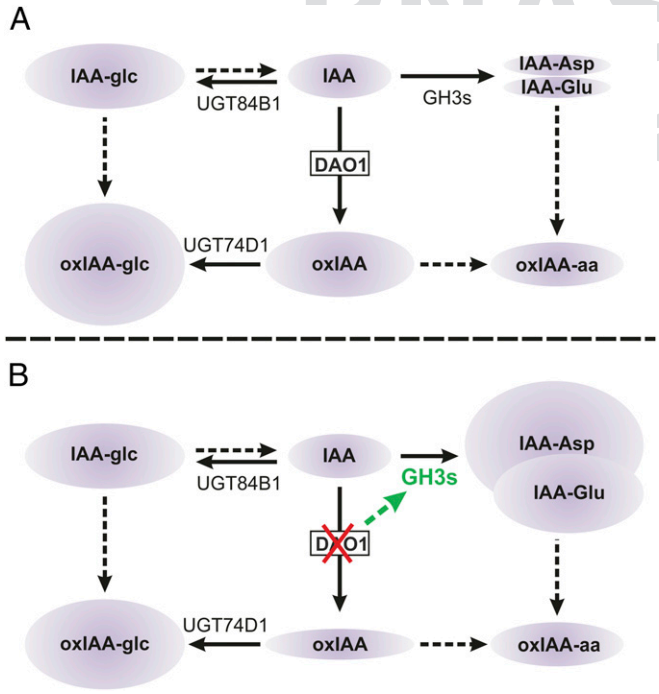

Fig. 5. IAA degradation and conjugation regulate IAA homeostasis in *Arabidopsis*. (*A*) In WT plants, IAA is irreversibly oxidized to oxIAA by DAO1 and subsequently conjugated with glucose by the UGT74D1 enzyme to produce oxIAA-glc (9). IAA can also be conjugated to either glucose (IAA-glc) or amino acids by UGT84B1 (7) and members of the GH3 family (2), respectively. IAA-Glu and IAA-Asp are the most abundant IAA-amino acid conjugates in *Arabidopsis* (5, 10, 11) and believed to be irreversible conjugates that cannot be hydrolyzed to form free IAA (4, 10). (*B*) In the *dao1-1* mutant, *GH3* genes are up-regulated to drain accumulating IAA by irreversible conjugation to form IAA-Asp and IAA-Glu, whereas IAA-glc levels are unaltered. Solid arrows indicate steps in which the indicated enzyme is known to catalyze the reaction. Dashed arrows indicate steps that are not well-defined. oxIAA-aa, 2-oxoindole-3-acetic acid amino acid.

Root Phenotyping. The number of lateral roots per seedling was counted using a stereo microscope, and digital images were taken. For RH measurements, seedlings were imaged with a camera mounted to a Leica stereomicroscope. The digital images were used for RH and primary root length measurement with FIJI software. RHs ∼3 mm from the root tip were measured (10 RHs per seedling). For hormone treatment, the indicated concentration of IAA was added to 1/2 Murashige and Skoog medium before it solidified. For gravitropic response assays, plates containing 6-d-old seedlings grown on a 12-h/12-h light/dark period were turned 90°, and the root angle was imaged every 60 min for 8 h using an automated image acquisition system (23) and quantified using FIJI software.

Cloning of At1g14130 and *Arabidopsis* Transformation. The transcriptional and translational fusions as the overexpression lines of At1g14130 were generated in gateway-compatible vectors. Genomic DNA from Col-0 was used to amplify 847 bp upstream of the At1g14130 translational start codon by using the At1g14130pro forward and reverse primers (Table S1). The PCR product was cloned into pENTR-D-Topo entry vector (Invitrogen) and recombined by LR reaction into the pGWB3 destination binary vector to create a transcriptional GUS fusion. For the translational fusion, a fragment of 1,846 bp, containing the At1g14130 promoter and coding sequence region without the stop codon, was amplified with At1g14130gfp primers (Table S1). The PCR product was cloned into pENTR-D-Topo entry vector (Invitrogen) and recombined by LR reaction into the pGWB4 (24) destination binary vector to create a translational GFP fusion. To create an overexpression line, the coding sequence of At1g14130 was amplified using the At1g14130cds primers (Table S1). The PCR product was cloned into pENTR-D-Topo entry vector (Invitrogen) and recombined by LR reaction into the pK2GW7 (24) destination binary vector. The authenticity of all constructs was verified by sequencing before transformation. *A. thaliana* (ecotype Columbia) plants were transformed with *Arabidopsis tumefaciens* (strain GV3101) using the floral dipping method (25). Screening of T3 seeds for 100% antibiotic resistance identified homozygous plants for the transgene.

IAA Metabolite Profiling. *A. thaliana* WT Col-0 as well as *gh3.1,2,3,4,5,6* and *dao1* mutant lines were grown under LD conditions for 7 or 10 d. Whole seedlings or dissected tissues were collected in five replicates (20 mg tissue per sample). Sample purification and quantification of IAA metabolites were performed as described in ref. 11.

Feeding Experiments with Labeled IAA and Indole. Seven-day-old *Arabidopsis* seedlings (Col-0, *gh3.1,2,3,4,5,6*, and *dao1* mutant lines) were incubated with liquid medium containing 0.5 μM [$^{13}C_6$]IAA or 10 μM [$^{15}N_1$]indole for 0, 3, 6, 12, and 24 h under gentle shaking and in darkness. For each time point, 20 mg whole seedlings were collected in three replicates. The samples were extracted and purified by solid-phase extraction as described in ref. 11. Incorporation of the label into IAA metabolites was measured using LC-MS/MS, with the Multiple Reaction Monitoring transitions corresponding to endogenous and labeled compounds. De novo synthesis of IAA metabolites was expressed as the concentration of labeled metabolites at individual time points after correction for natural isotope abundances (26).

Microscopy. Confocal microscopy was performed using a Leica SP5 Confocal Laser-Scanning Microscope (Leica Microsystems). Cell walls were stained using propidium iodide (10 μg/mL; Sigma). Scanning settings used for one experiment were optimized and kept unchanged throughout the experiment. Images were processed using the Leica SP5 Image Analysis software. Images for Fig. 2 were processed with Adobe Photoshop only for adjustment of brightness and contrast.

Histochemical Analysis. The GUS gene activity was revealed by incubating seedlings at 37° for 1 h in a phosphate buffer (500 mM; pH 7) containing

0.5 mM potassium ferricyanide, 0.5 mM potassium ferrocyanide, 1 mM EDTA (pH 8), 0.5% (vol/vol) Triton X-100, and 1 mM 5-bromo-4-chloro-3-indolyl β-D-glucuronide (X-Gluc; Sigma). The X-Gluc was initially dissolved in dimethylformamide to reach a final concentration of 0.5%. After GUS staining, seedlings were cleared and mounted in 50% (wt/vol) glycerol.

qRT-PCR. Real-time qRT-PCR reactions were performed on a LightCycler 480 apparatus (Roche) using SYBR Green Master Mix (Bioline). A standard reaction mixture (12 μL) contained 5 μL cDNA template, 6 μL 2× SYBR Green I Master Mix (Roche), 0.1 μL 100 μM forward and reverse primers, and 0.8 μL H_2O. All of the specific primer pairs (Table S1) were designed with the Universal Probe Library Assay Design Center (Roche; lifescience.roche.com/shop/home) and used to quantify the gene expression levels. *Arabidopsis ACT2* gene (At3g18780) was used as a constitutive internal standard, which showed no clear changes in *Cycle threshold* values, to normalize the obtained gene expression results. All individual reactions were done in triplicates.

ACKNOWLEDGMENTS. We thank the Swedish Metabolomics Centre for the use of instrumentation. S.P. and M.J.B. acknowledge PhD scholarship support from the University of Nottingham. This work was funded by Ministry of Education, Youth and Sport of the Czech Republic National Program for Sustainability I Grant LO1204 and Internal Grant Agency of Palacky University Grant IGA_PrF_2016_011 (to A.P., P.P., and O.N.). A.R. and M.J.B. acknowledge support of the Saudi Arabian Ministry of Higher Education. U.V., A.B., R.S. and M.J.B. acknowledge support of the Biological and Biotechnology Science Research Council Responsive Mode and CISB awards to the Centre for Integrated Structural Biology. R.C.-S., A.P., O.N., and K.L. acknowledge support from the Swedish Foundation for Strategic Research, the Swedish Research Council, Carl Tryggers Stiftelse för Vetenskaplig Forskning, and Kempestiftelserna. A.G. and K.V. were supported by Research Foundation Flanders Grants G009412N, G.0.602.11.N.10, and 1.5.091.11.N.00 and University of Antwerp Grant BOF-DOCPRO4. K.S. and M.J.B. acknowledge support of the European Research Council FUTUREROOTS Project. P.H. and A.L.P. are funded by the 20:20 Wheat Institute Strategic Programme Grant from the Biotechnology and Biological Sciences Research Council of the United Kingdom.

1. Ludwig-Müller J (2011) Auxin conjugates: Their role for plant development and in the evolution of land plants. *J Exp Bot* 62(6):1757–1773.
2. Staswick PE, et al. (2005) Characterization of an Arabidopsis enzyme family that conjugates amino acids to indole-3-acetic acid. *Plant Cell* 17(2):616–627.
3. Westfall CS, Herrmann J, Chen Q, Wang S, Jez JM (2010) Modulating plant hormones by enzyme action: The GH3 family of acyl acid amido synthetases. *Plant Signal Behav* 5(12):1607–1612.
4. Östin A, Kowalyczk M, Bhalerao RP, Sandberg G (1998) Metabolism of indole-3-acetic acid in Arabidopsis. *Plant Physiol* 118(1):285–296.
5. Kai K, Horita J, Wakasa K, Miyagawa H (2007) Three oxidative metabolites of indole-3-acetic acid from *Arabidopsis thaliana*. *Phytochemistry* 68(12):1651–1663.
6. Pencík A, et al. (2013) Regulation of auxin homeostasis and gradients in Arabidopsis roots through the formation of the indole-3-acetic acid catabolite 2-oxindole-3-acetic acid. *Plant Cell* 25(10):3858–3870.
7. Jackson RG, et al. (2001) Identification and biochemical characterization of an Arabidopsis indole-3-acetic acid glucosyltransferase. *J Biol Chem* 276(6):4350–4356.
8. Peer WA, Cheng Y, Murphy AS (2013) Evidence of oxidative attenuation of auxin signalling. *J Exp Bot* 64(9):2629–2639.
9. Tanaka K, et al. (2014) UGT74D1 catalyzes the glucosylation of 2-oxindole-3-acetic acid in the auxin metabolic pathway in Arabidopsis. *Plant Cell Physiol* 55(1):218–228.
10. Kowalczyk M, Sandberg G (2001) Quantitative analysis of indole-3-acetic acid metabolites in Arabidopsis. *Plant Physiol* 127(4):1845–1853.
11. Novák O, et al. (2012) Tissue-specific profiling of the *Arabidopsis thaliana* auxin metabolome. *Plant J* 72(3):523–536.
12. Butler ED, Gallagher TF (2000) Characterization of auxin-induced ARRO-1 expression in the primary root of Malus domestica. *J Exp Bot* 51(351):1765–1766.
13. Zhao Z, et al. (2013) A role for a dioxygenase in auxin metabolism and reproductive development in rice. *Dev Cell* 27(1):113–122.
14. Yi K, Menand B, Bell E, Dolan L (2010) A basic helix-loop-helix transcription factor controls cell growth and size in root hairs. *Nat Genet* 42(3):264–267.
15. Balcerowicz D, Schoenaers S, Vissenberg K (2015) Cell fate determination and the switch from diffuse growth to planar polarity in Arabidopsis root epidermal cells. *Front Plant Sci* 6:1163.
16. Velasquez SM, Barbez E, Kleine-Vehn J, Estevez JM (2016) Auxin and Cellular Elongation. *Plant Physiol* 170(3):1206–1215.
17. Datta S, Prescott H, Dolan L (2015) Intensity of a pulse of RSL4 transcription factor synthesis determines Arabidopsis root hair cell size. *Nat Plants* 1(10):15138.
18. Mellor N, et al. (2016) Dynamic regulation of AtDAO1 and GH3 modulates auxin homeostasis. *Proc Natl Acad Sci USA*, 10.1073/pnas.1604458113.
19. Ljung K (2013) Auxin metabolism and homeostasis during plant development. *Development* 140(5):943–950.
20. Zhang J, et al. (2016) Oxidative inactivation by DAO1 regulates growth in *Arabidopsis thaliana*. *Proc Natl Acad Sci USA*, 10.1073/pnas.1604769113.
21. Voß U, et al. (2015) The circadian clock rephases during lateral root organ initiation in *Arabidopsis thaliana*. *Nat Commun* 6:7641.
22. Park JE, et al. (2007) GH3-mediated auxin homeostasis links growth regulation with stress adaptation response in Arabidopsis. *J Biol Chem* 282(13):10036–10046.
23. Wells DM, et al. (2012) Recovering the dynamics of root growth and development using novel image acquisition and analysis methods. *Philos Trans R Soc Lond B Biol Sci* 367(1595):1517–1524.
24. Nakagawa T, et al. (2007) Development of series of gateway binary vectors, pGWBs, for realizing efficient construction of fusion genes for plant transformation. *J Biosci Bioeng* 104(1):34–41.
25. Clough SJ, Bent AF (1998) Floral dip: A simplified method for Agrobacterium-mediated transformation of *Arabidopsis thaliana*. *Plant J* 16(6):735–743.
26. Cobelli C, Toffolo G, Foster DM (1992) Tracer-to-tracee ratio for analysis of stable isotope tracer data: Link with radioactive kinetic formalism. *Am J Physiol* 262(6 Pt 1): E968–E975.

Supporting Information

Porco et al. 10.1073/pnas.1604375113

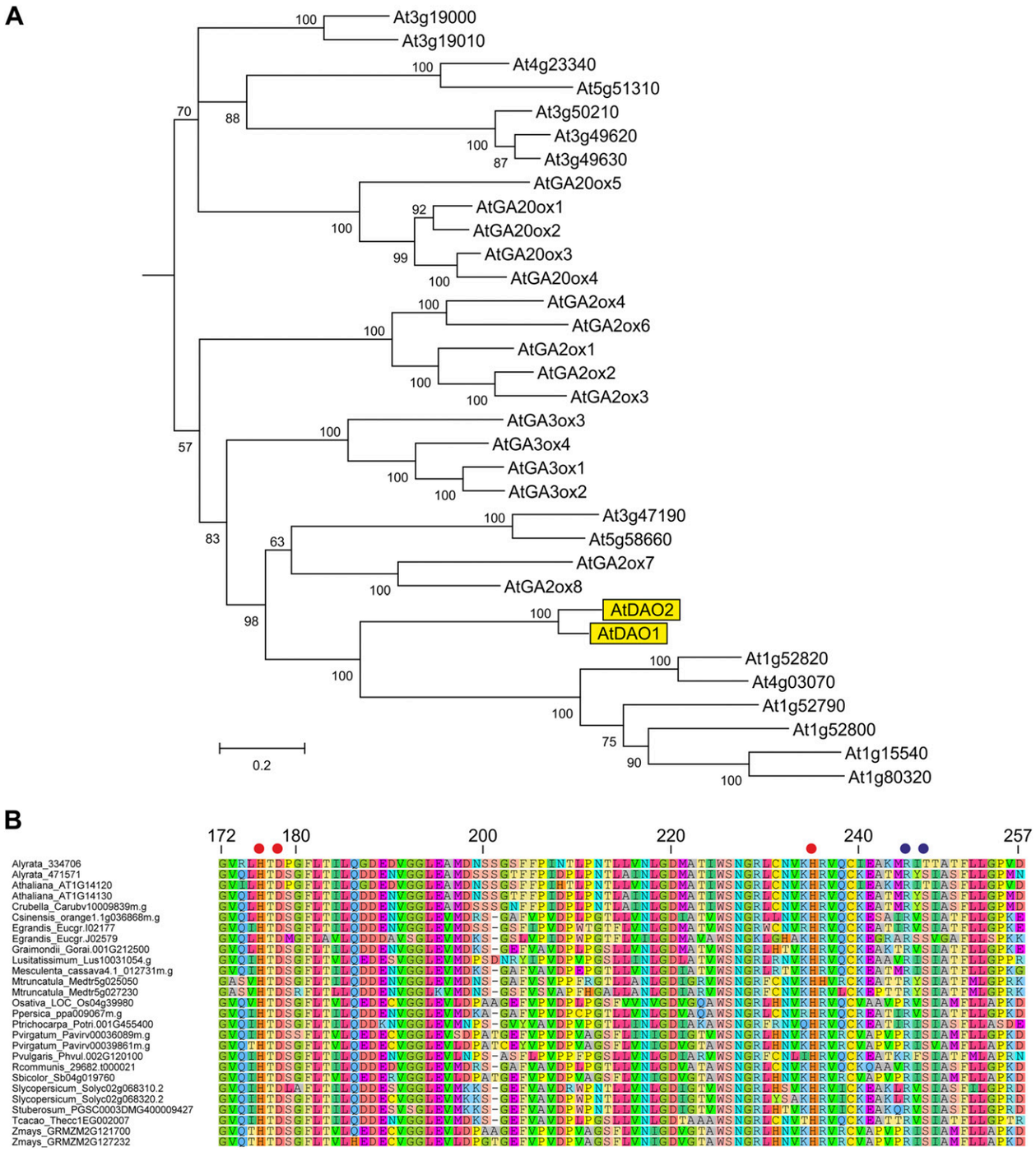

Fig. S1. Phylogenetic relationships between AtDAOs and related proteins. (*A*) Phylogenetic tree of the AtDAO1 and AtDAO2 and related *Arabidopsis* proteins. *Arabidopsis* 2-ODD sequences were aligned using MUSCLE within Geneious and trimmed to remove unaligned residues. Phylogenetic analysis was carried out using PhyML and MrBayes within ToPALI (www.topali.org/). A section of the MrBayes tree was selected and displayed in MEGA6. Numbers show branch support values; the scale bar shows substitutions per site. (*B*) Sequence alignment of the active site region of AtDAOs and related proteins from various plant species identified at https://phytozome.jgi.doe.gov/pz/portal.html. Sequences were aligned using MUSCLE. The Fe binding residues are indicated with red dots, and the 2-oxoglutarate binding residues are indicated with blue dots. Residue numbering is from the AtDAO1 (At1g14130) sequence.

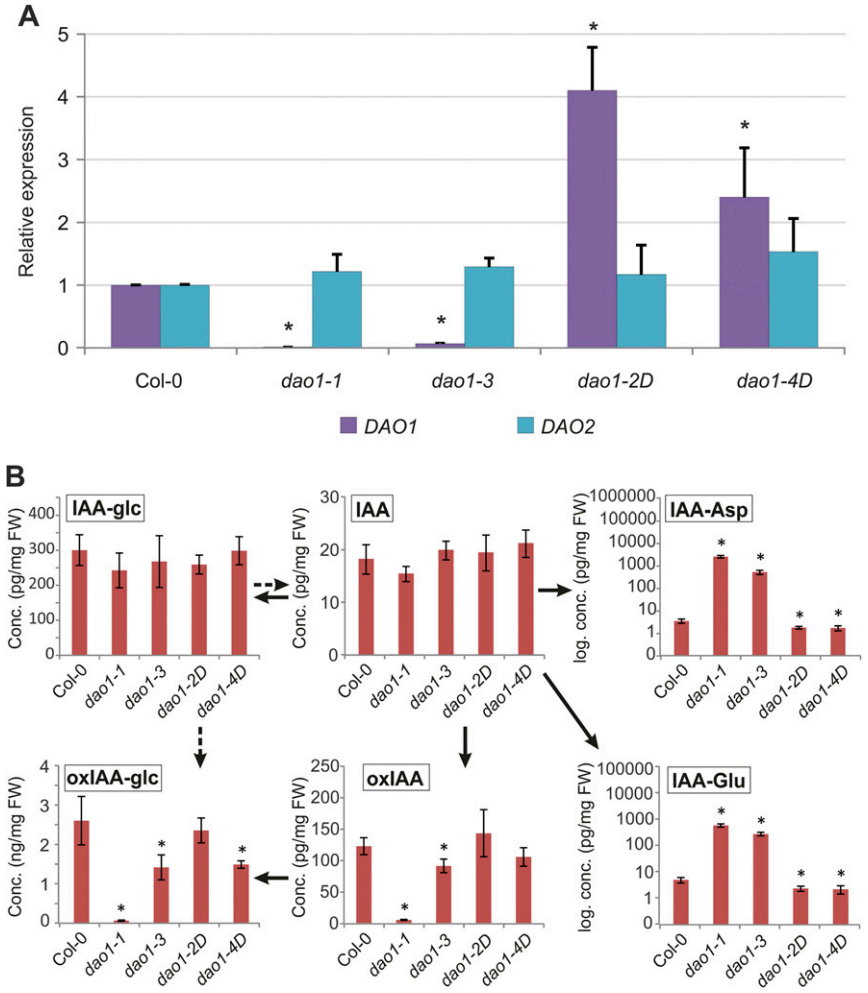

Fig. S2. (*A*) *AtDAO1* and *AtDAO2* transcript abundance in the different *dao1* alleles studied in this work relative to Col-0. qRT-PCR analysis was performed using cDNA from 7-d-old roots. Fold change was calculated by comparative *Cycle threshold* (*Ct*) method, and values were normalized with the expression of the *ACT2* gene. Error bars indicate SDs from three biological replicates. *Expression values significantly different from those in Col-0 (Student's *t* test; $P < 0.05$). (*B*) Levels of IAA metabolites in the different *dao1* alleles. IAA and the metabolites oxIAA, oxIAA-glc, IAA-glc, IAA-Asp, and IAA-Glu were quantified in 7-d-old seedlings of Col-0, *dao1-1*, *dao1-3*, *dao1-2D*, and *dao1-4D*. The concentrations for all metabolites except oxIAA-glc [nanograms per milligram fresh weight (FW)] are given in picograms per milligram FW. Samples were analyzed in five independent biological replicates, and error bars represent the SDs. *Statistically significant differences from Col-0 ($P < 0.05$; Student's *t* test).

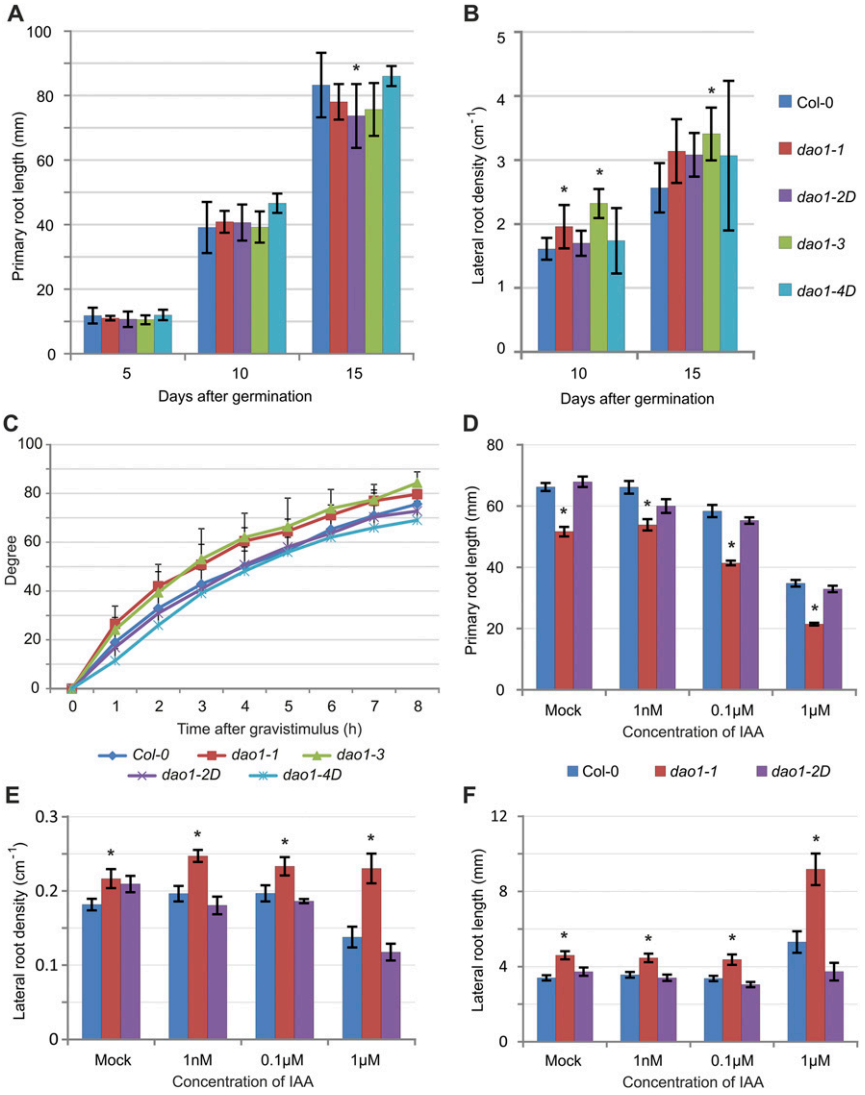

Fig. S3. Root phenotypes of the *dao1* mutant alleles. (*A*) Primary root length and (*B*) lateral root density of *dao1* mutants over the vegetative phase. *Values significantly different from those in Col-0 (Mann–Whitney *U* test; $P < 0.05$; $n = 10$). (*C*) Gravitropic response of the *dao1* mutants measured from 6-d-old seedlings ($n = 20$). (*D–F*) Effect of IAA on (*D*) primary root length, (*E*) lateral root density, and (*F*) lateral root length in 10-d-old *dao1-1* and *dao1-2D* mutants. Error bars indicate SD. *Values significantly different from those in Col-0 (Student's *t* test; $P < 0.05$; $n > 12$).

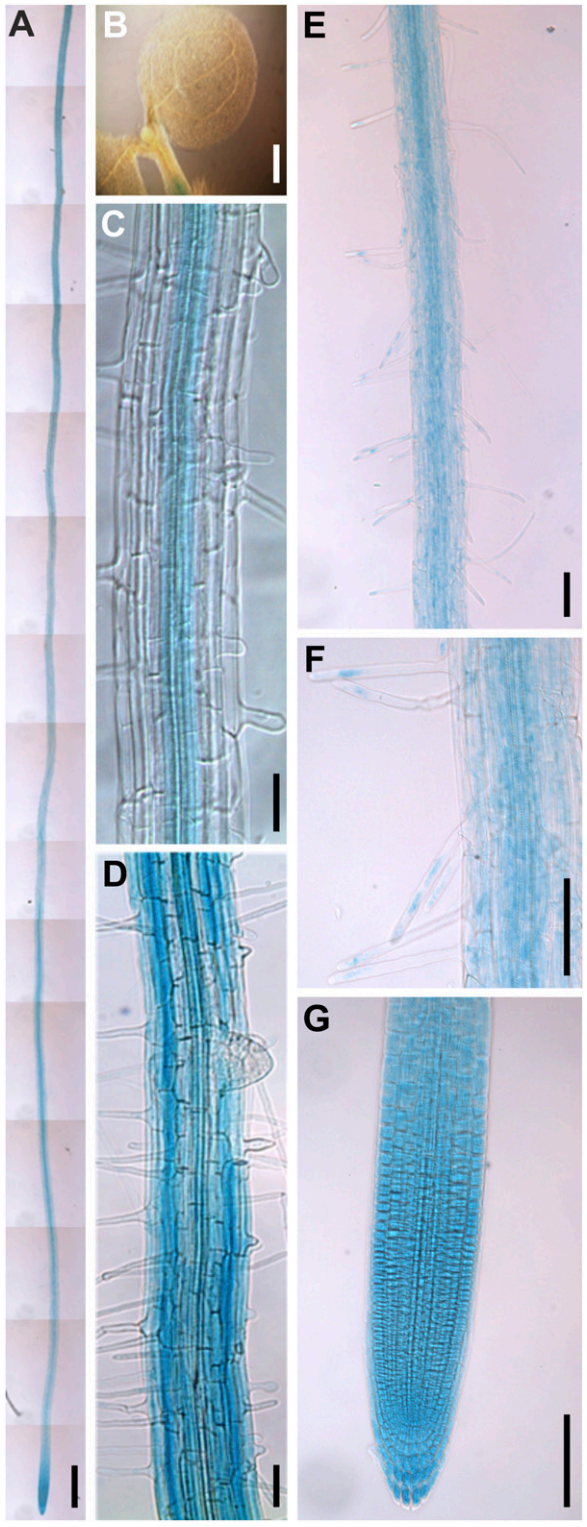

Fig. S4. DAO1 promoter is mainly active in roots. Visualization of *pDAO1:GUS* activity in (*A*) the root, (*B*) the aerial portion, (*C*) the stele, (*D*) epidermal cells in the mature part of the root, (*E* and *F*) RHs, and (*G*) the root tip. Pictures were taken from (*A* and *E*–*G*) 7-, (*B*) 4-, and (*C* and *D*) 5-d-old seedlings. (Scale bars: *A*, 500 μm; *B* and *E*–*G*, 100 μm; *C* and *D*, 50 μm.)

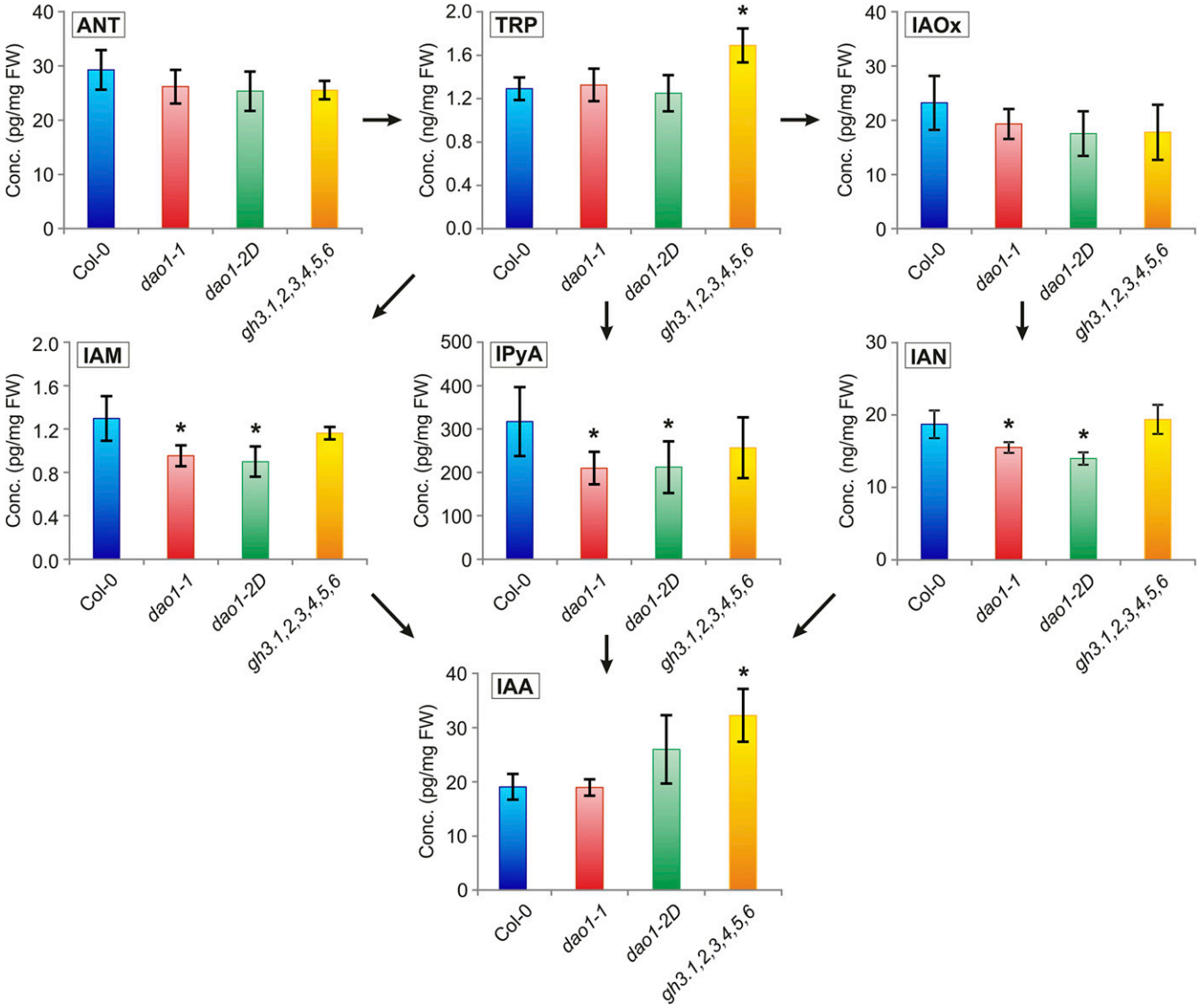

Fig. S5. Levels of IAA precursors in IAA oxidase and GH3 mutant backgrounds. IAA and the IAA precursors [anthranilate (ANT), indole-3-acetaldoxime (IAOx), indole-3-acetamide (IAM), indole-3-pyruvic acid (IPyA), and indole-3-acetonitrile (IAN)] were quantified in 7-d-old seedlings of Col-0, *dao1-1*, *dao1-2D*, and the *gh3* sextuple mutant line *gh3.1,2,3,4,5,6*. The concentration is given in picograms per milligram fresh weight (FW), except for TRP and IAN (nanograms per milligram FW). Samples were analyzed in five independent biological replicates, and error bars represent SDs. *Statistically significant differences from Col-0 ($P < 0.05$; Student's *t* test).

Fig. S6. Seedlings from the Col-0 WT and the *dao1-1* and *gh3.1,2,3,4,5,6* mutant lines. Pictures were taken 7 and 14 d after germination (dag). (Scale bars: 5 mm.)

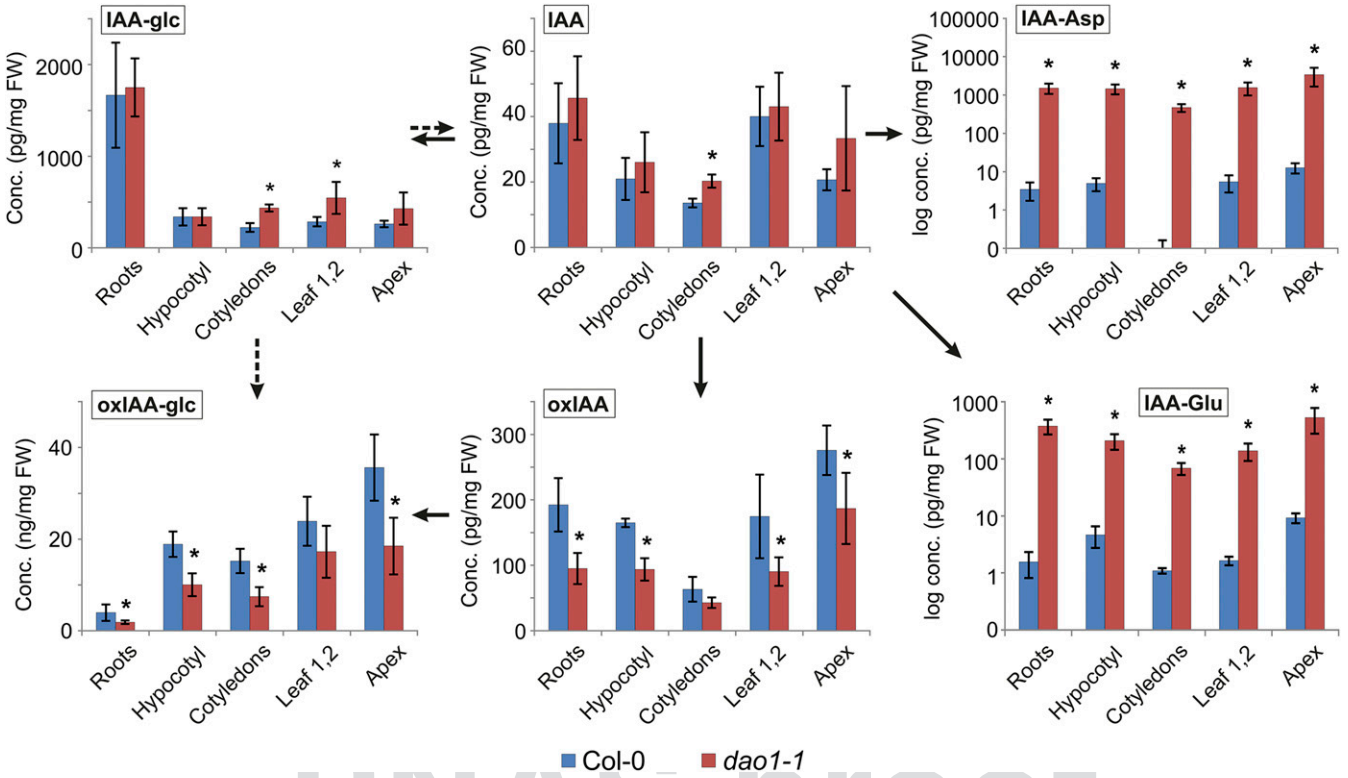

Fig. S7. Levels of IAA metabolites in different tissues of WT Col-0 and *dao1-1* seedlings. IAA and the IAA metabolites oxIAA, oxIAA-glc, IAA-glc, IAA-Asp, and IAA-Glu were quantified in root, hypocotyl, cotyledons, leaves 1 and 2, and shoot apex tissues from 10-d-old Col-0 (blue) and *dao1-1* mutant (red) seedlings. The concentrations for all metabolites are given in picograms per milligram fresh weight (FW) or nanograms per milligram FW (IAA-Asp and IAA-Glu are given in log scale). Samples were analyzed in five independent biological replicates, and error bars represent SDs. *Statistically significant differences from Col-0 ($P < 0.05$; Student's *t* test).

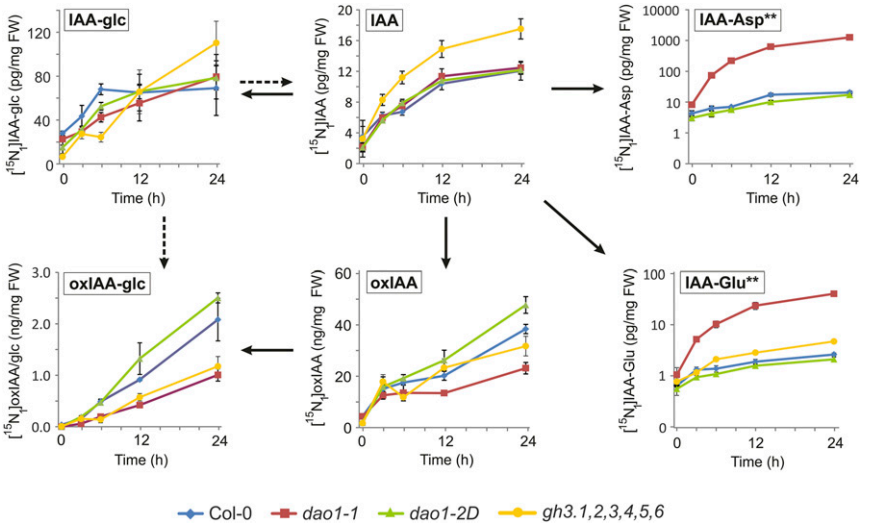

Fig. S8. In vivo labeling of IAA and IAA metabolites after feeding with [$^{15}N_1$]indole. Seven-day-old Col-0, *dao1-1*, *dao1-2D*, and *gh3.1,2,3,4,5,6* seedlings were incubated with [$^{15}N_1$]indole, and the levels of IAA and IAA metabolites were quantified after different times of incubation. The level of [$^{15}N_1$]IAA-Asp in the *gh3.1,2,3,4,5,6* mutant line was under the detection limit of the used LC-MS/MS method. The levels of de novo synthesized metabolites are given in picograms per milligram fresh weight (FW) or nanograms per milligram FW; $n = 3$. Error bars indicate SD. **Concentrations are given in log scale.

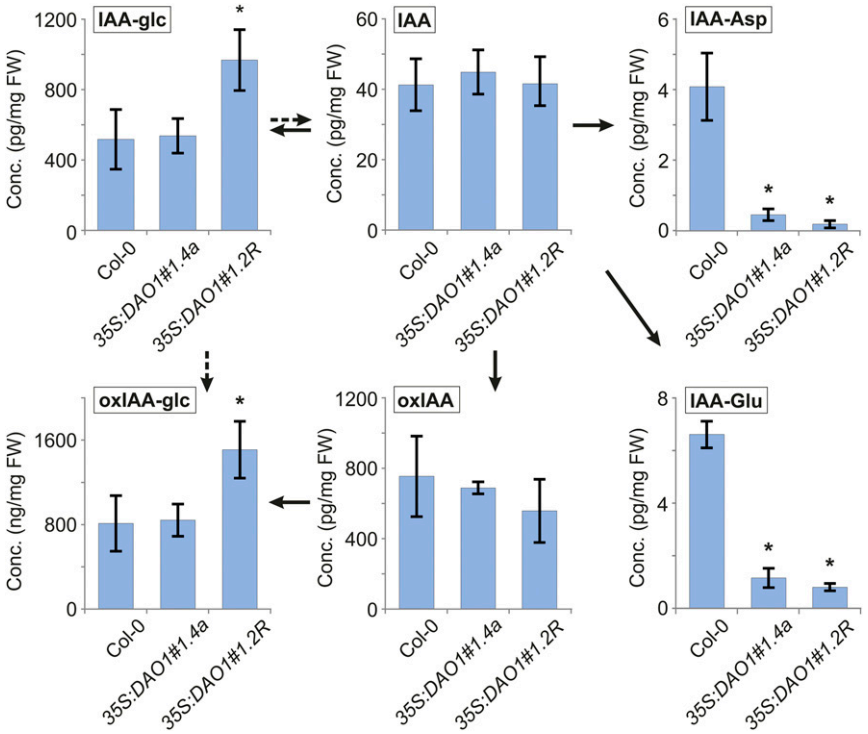

Fig. S9. Levels of IAA metabolites in IAA oxidase overproducing lines. IAA and the metabolites oxIAA, oxIAA-glc, IAA-glc, IAA-Asp, and IAA-Glu were quantified in 7-d-old seedlings of Col-0 and two independent *35S:DAO1* lines (*35S:DAO1#1.4a* and *35S:DAO1#1.2R*). The concentrations for all metabolites except oxIAA-glc [nanograms per milligram fresh weight (FW)] are given in picograms per milligram FW. Samples were analyzed in five independent biological replicates, and error bars represent the SDs. *Statistically significant differences from Col-0 ($P < 0.05$; Student's *t* test).

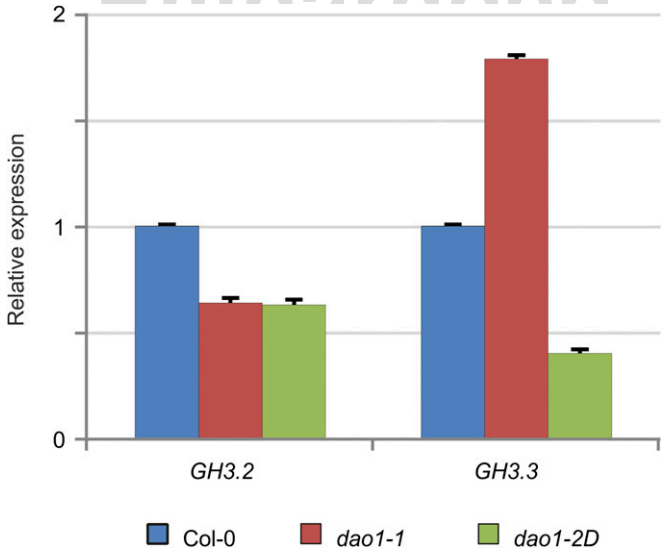

Fig. S10. *GH3* transcript abundance in the *dao1-1* and *dao1-2D* mutants relative to Col-0. qRT-PCR analysis was performed using cDNA from 7-d-old roots. Fold change was calculated by comparative *Ct* method, and values were normalized with the expression of the *ACT2* gene. Error bars indicate SDs.

Table S1. Primers used in this work

Purpose and primer name	Primer sequence (5′→3′) Forward primer	Reverse primer
Genotyping of insertion lines		
dao1-1	TTCCCCACGGAATTAAG GTAC	CTATGGGGAAAAAGGTTCC TG
dao1-2D	AGCGGTTTGAG ATAC ATGTGG	TTGGTGGACTTG AAGC TATGG
dao1-3	TGAAACATCCCC ATC TCTC AC	ATAAATTTG GGCCC AAAAGTG
dao1-4D	TCCGTTTAGTTCCCCC ATATC	TCGTGTTTTGGG TCTC CTATG
Gh3.3	GTGACAGGCAG AG TCACAAG C	TTTTAACGTATTAATC TTGGC ACG
Gh3.4	CAATGACGGGATTTTGATC AC	TGTGGAGCGGAATTATG AAAC
Gh3.5	AGGCCAGTGTTG TTGTC TTTG	TGGTCTTGAGCATAG ATTCCG
Gh3.6	GCAAAAACAGC ACC AAC ACG A	CGCAGCTTTGGAG GTTTC TG A
LBb3.1	ATTTTGCCGATTTC GG AAC	
LB1	GCCTTTTCAGAAATGG ATAAATAG CCTT GCTTCC	
Lba1	TGGTTCACGTAG TG GGCC ATCG	
3′dSpm	TACGAATAAGAGCG TCC ATTTTAG AGT	
Cloning		
At1g14130pro	CACCTTCCATAGAAATGTATATG TG	ATCTTCAATGG AG AG GTTAAC
At1g14130gfp	CACCTTCCATAGAAATGTATATG TG	TTTATCTAGTCC TGC ATGG G
At1g14130cds	CACCATGGGGGAACTAAACG G	TCATTTATCTAGTC CTG CATG
qRT-PCR		
qDAO1	TCGAAGCTTCTGC AG ATCAA	TTTCCTCGCTAAATCC GTTG
qDAO2	CCAGTGGATAG AG ATCTTG AAGC	GGCTTGTATAG TCGC GG ATG
qGH3.2	GTTTGCTTCCGGTC TCCTC	CACGAGCAAGTTCCTTCC A
qGH3.3	CATCACAGAGTTCCTC AC AAGC	GTCGGTCCATGTCTTC ATC A
qRSL4	TCTCTTGGGGATGTTCAAC TTT	AGGCCAAGCAAC TCG TCTC
qACT2	CCGCTCTTTCTTTCCAAGC	CCGGTACCATTGTC AC AC AC